Mon. Not. R. Astron. Soc. **372,** 1117–1128 (2006) doi:10.1111/j.1365-2966.2006.10913.x

The SuperWASP wide-field exoplanetary transit survey: candidates from fields 23 h < RA < 03 h

D. J. Christian,[1⋆] D. L. Pollacco,[1] I. Skillen,[2] R. A. Street,[1] F. P. Keenan,[1] W. I. Clarkson,[3] A. Collier Cameron,[4] S. R. Kane,[4] T. A. Lister,[4,6] R. G. West,[5] B. Enoch,[3] A. Evans,[6] A. Fitzsimmons,[1] C. A. Haswell,[3] C. Hellier,[6] S. T. Hodgkin,[7] K. Horne,[4] J. Irwin,[7] A. J. Norton,[3] J. Osborne,[5] R. Ryans,[1] P. J. Wheatley[8] and D. M. Wilson[6]

[1]*Astrophysics and Planetary Science Research Division, Department of Physics and Astronomy, Queen's University Belfast, Belfast BT7 1NN*
[2]*Isaac Newton Group of Telescopes, Apartado de correos 321, E-38700 Santa Cruz de la Palma, Tenerife, Spain*
[3]*Department of Physics & Astronomy, The Open University, Milton Keynes MK7 6AA*
[4]*School of Physics & Astronomy, University of St. Andrews, North Haugh, St. Andrews, Fife KY16 9SS*
[5]*Department of Physics & Astronomy, University of Leicester, Leicester LE1 7RH*
[6]*Astrophysics Group, School of Chemistry & Physics, Keele University, Staffordshire ST5 5BG*
[7]*Institute of Astronomy, University of Cambridge, Madingley Road, Cambridge CB3 0HA*
[8]*Department of Physics, University of Warwick, Coventry CV4 7AL*

Accepted 2006 August 3. Received 2006 August 3; in original form 2006 July 3

ABSTRACT

Photometric transit surveys promise to complement the currently known sample of extra-solar planets (ESPs) by providing additional information on the planets and especially their radii. Here, we present ESP candidates from one such survey called, the Wide Angle Search for Planets (WASP) obtained with the SuperWASP wide-field imaging system. Observations were taken with SuperWASP North located in La Palma during the 2004 April to October observing season. The data cover fields between 23 and 03 h in RA at declinations above +12. This amounts to over ≈400 000 stars with V magnitudes 8–13.5. For the stars brighter than 12.5, we achieve better than 1 per cent photometric precision. Here, we present 41 sources with low-amplitude variability between ≈1 and 10 mmag, from which we select 12 with periods between 1.2 and 4.4 d as the most promising ESP candidates. We discuss the properties of these ESP candidates, the expected fraction of transits recovered for our sample and implications for the frequency and detection of hot-Jupiters.

Key words: methods: data analysis – planetary systems formation – stars: variables: other.

1 INTRODUCTION

The discovery of the large debris disc around β Pic (Smith & Terrile 1984) and other young stellar sources with discs (Lecavelier Des Etangs et al. 1997; Jayawardhana et al. 1998), plus the subsequent discovery of numerous extra-solar planets (ESPs), has led to a resurgence in the study of planet and Solar system formation. Discoveries of ESPs have been dominated by radial velocity (RV) surveys (Mayor & Queloz 1995; Marcy & Butler 1998, 2000; Udry et al. 2000). Currently, there are over 170 known ESPs orbiting around over 150 host stars. Photometric transit surveys have identified about 10 new planets, starting with the confirmation of the first system, HD 209458b (Henry et al. 2000; Charbonneau et al. 2000), followed by several discovered with the Optical Gravitational Lensing Experiment (OGLE) project and confirmed with RV follow-up (Konacki et al. 2003, 2004; Pont et al. 2004; Bouchy et al. 2005a; Konacki et al. 2005), to the discovery of TrES 1 (Alonso et al. 2004), the detection of the transits from the RV discovered HD 189733 (Bouchy et al. 2005b), and the recent discovery and follow-up of XO-1b (McCullough et al. 2006; Wilson et al. 2006; Holman et al. 2006). These planets typically have periods less than 4 d, orbital distance of ∼0.05 au and Jupiter-like masses and radii, and hence have been called the *hot-Jupiters*. Additionally, several very short period (P < 1.5 d) systems have been discovered (Konacki et al. 2003; Bouchy et al. 2004) and termed *very-hot-Jupiters*.

RV surveys measure the Doppler velocity of individual stars at many different times, which is a very time consuming procedure. The photometric transit method can measure thousands of stars simultaneously. In addition to monitoring a large number of stars, photometric transit detections provide information on the planet's

⋆E-mail: d.christian@qub.ac.uk

radius and inclination, not readily available from RV surveys. It is currently not know what fraction of stars contain planets. The fraction of planets that may be hot-Jupiters is also not known. About 20 per cent of the currently known ESPs have periods less than 10 d (Butler et al. 2006) and ≈10–15 per cent of solar-type stars surveyed have ESPs (Lineweaver & Grether 2003). There have been several attempts to better define what percentage of stars has planets. These range from 1–2 per cent (Brown 2003) to 20 per cent (Lineweaver & Grether 2003), but the latter also speculate this may be a lower limit. The large number of stars covered by photometric transit surveys should provide better constraints on the fraction of stars with hot-Jupiters, and may shed light on their formation mechanisms.

Here, we present results from one such photometric transit survey, called the Wide Angle Search for Planets (WASP). WASP consists of two separate telescopes, called SuperWASP North (SW-N) and SuperWASP South (SW-S). The SuperWASP (SW) telescopes were designed to cover a large field of view with better than 1 per cent photometric accuracy down to 12th magnitude. Each SW telescope consists of eight separate cameras, each of which covers 61 deg^2 of sky, and the combined system surveys nearly 500 deg^2. The results presented here are from the 2004 SW-N observing campaign taken with a five-camera configuration. A description of the SW instruments and observing strategy is presented in Section 2. In Section 3, we present the data reduction and analysis techniques for the ESP search. Candidates with secure low-amplitude variability that may be ESPs are presented in Section 4. In Section 5, we discuss possible false alarms, expected fraction of recovered transits and indications for the frequency of hot-Jupiters, their properties and observing follow-up strategies to confirm the transits planetary nature. Lastly, in Section 6 we summarize our findings.

2 INSTRUMENTATION AND OBSERVATIONS

2.1 Instrumentation

The SW telescopes were designed to cover a large area of sky and achieve photometric accuracy of a few mmag and improve on the success of the prototype WASP0 instrument (Kane et al. 2004, 2005). SW-N in La Palma is contained in its own custom enclosure with a hydraulically operated roll-away roof, and its own Global Positioning System (GPS) and weather station (Pollacco et al. 2006). The telescope mount is a rapid slew fork mount (≈10° s^{-1}) from Optical Mechanics Incorporated. Commercially available components were used where available to keep costs down and reduce construction time. These components include: the telescope control system (TCS), a dedicated PC for each camera for data acquisition and a PC attached to a digital linear tape (DLT) autoloader for data storage. The TCS monitors the weather, sets time for the Flexible Image Transport System (FITS) data header from the GPS and can close the roof in the event of a weather alert (Pollacco et al. 2006). All major components are run with Linux OS.

To meet the science requirements of covering a large area of sky with high photometric precision, a combination of Canon 200-mm f/1.8 lenses and Andor e2v 2 × 2 k back illuminated CCDs was chosen. The CCDs are passively cooled with a Pelletier cooler and have a very short 4-s readout time. This combination of lens and camera gives a field of 7.°8 × 7.°8 (∼61 deg^2). No additional filters were used, and this 'wide-*V*' set-up covers from 8 to 15 mag for a typical 30-s exposure. A < 1 per cent photometric precision was obtained for magnitudes brighter than $V = 12.5$. Additional details of the SW project and instrumentation is presented in Pollacco et al. (2006).

2.2 Observational strategy

SW-N was commissioned in 2003 November, and inaugurated on 2004 April 16. Our initial observing strategy was tailored towards searching for ESP transits. This was to observe fields with a large number of stars, but to avoid the Galactic plane where over-crowded fields would increase the number of blended stars and make detection and data reduction difficult. Based on the Besancon Galactic model (Robin et al. 2003), a declination of +28 was chosen, with the telescope stepping through RA in 1 h increments centred on the current Local Sidereal Time (LST), but within the ±4.5 h hour angle limit of the mount. A maximum of eight fields were observed with a duration of ≈1 min per field, including a 30-s exposure, 4-s read-out and the time for the telescope to slew and settle at the new field. Such observations provide well-sampled light curves with a cadence of better than 8 min between subsequent measurements. This observing strategy provides a nightly baseline of over 6 h of coverage for the six fields centred near LST at midnight, and over 4 h of coverage on ≈10 fields per night. A typical field contains ∼20 000 stars per camera at magnitudes brighter than 13. Nightly calibrations, such as bias levels, darks and flat-fields to remove the pixel-to-pixel variations and vignetting, were obtained using automated scripts. Biases and flat-fields were obtained at the beginning and end of each night, and flat-fields were taken during twilight with the telescope pointed at zenith and the drive off. Exposure times were initially based on the data in Tyson & Gal (1993) and adjusted from the counts in the first image.

The ≈150 nights from the 2004 observing season covered several dozen separate fields and resulted in the detection of slightly more than 6.7 million stars. For the ESP search, these observations were separated into six equal sections of the sky, each containing about 1 million stars. This work presents the stars from 23 h < RA < 03 h, and contains nearly 900 000 stars observed for at least 25 nights and ≈400 image frames. The statistics for the observed fields are presented in Table 1, and the distribution of all stars in our sample as

Table 1. Field statistics.

Field SWASP	Nights	Images	Stars
J2317+2326	115	4882	38993
J2343+3126	112	4569	51694
J2344+2427	92	3406	38332
J2344+3944	110	4539	59202
J0016+3126	111	4525	48448
J0017+2326	110	4501	36676
J0043+3126	29	406	38458
J0044+2127	61	2046	30156
J0044+2427	29	406	34267
J0044+2826	80	3088	40578
J0045+3644	80	3061	46856
J0115+2826	79	3063	33249
J0116+2027	78	3051	27183
J0116+3126	28	372	34276
J0117+2326	27	371	28312
J0143+3126	72	2591	36623
J0144+2427	52	1576	28059
J0144+3944	71	2570	56242
J0216+3126	71	2560	40368
J0217+2326	70	2559	30535
J0243+3126	61	1883	40191
J0244+2427	42	1017	28958
J0244+3944	60	1879	78643

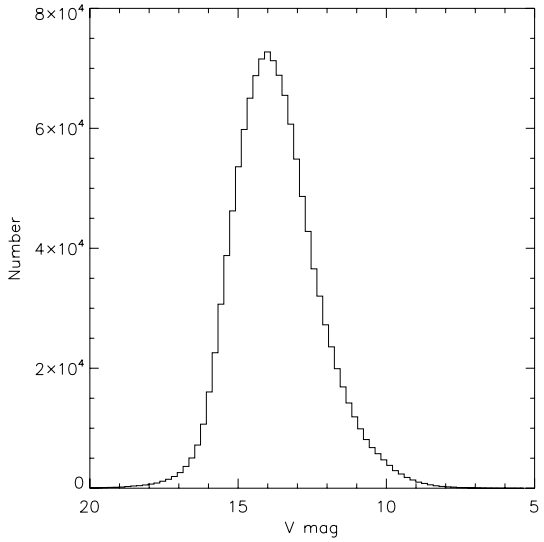

Figure 1. Distribution of stars in our sample (23 < RA < 03 h) as a function of *V* magnitude.

a function of SW-N *V* magnitude is shown in Fig. 1. Approximately 400 000 stars are brighter than 13.5 mag.

3 ANALYSIS

3.1 Pipeline

We have constructed a custom data reduction pipeline, with the goal of obtaining mmag photometric precision for stars with $V \leqslant 12$. The pipeline (only briefly described here) uses custom FORTRAN programs combined with shell scripts and several STARLINK packages, and creates master biases, darks and flat-fields for each night of observations. Flat-field calibration frames from individual nights are combined into a master flat using an exponential weighting with the contribution of flats older than 14 d diminishing (Collier-Cameron et al. 2006). Each science exposure is bias subtracted, dark corrected, flat-fielded, and the astrometric solution is computed using reference stars from the USNO-B1.0 and Tycho catalogues.

Aperture photometry is performed on the final calibrated images with a custom-built package tailored to deal with the ultra-wide fields. Bad pixel masks are applied to each frame, and a blending index is assigned for every object detected. The blend index is defined as the ratios of the fluxes in various-sized apertures for an individual star (Pollacco et al. 2006). We define two blend indices based on the flux ratios: $r_1 = (f_3 - f_1)/f_1$ and $r_2 = (f_3 - f_2)/f_2$, where f_1, f_2 and f_3 are the fluxes measured in apertures of 2.5, 3.5 and 4.5 pixels, respectively. Removing night-to-night variations in airmass and sky conditions was difficult, but the aperture photometry does achieve slightly better than the required 1 per cent precision at $V = 12.5$. For the transit searching, additional systematic errors are removed with the *SysREM* algorithm (Tamuz, Mazeh & Zuckerm 2005). rms precision as a function of SW *V* magnitude is shown in Collier-Cameron et al. (2006) and Pollacco et al. (2006). Fluxes are computed in the three, mentioned above, apertures and output, along with other source attributes to a FITS binary table. The final pipeline data products include the calibrated images, catalogue information and time-tagged photometric data for each star. Trends (such as extinction) are removed from the data, and the binary table is ingested by the archive. A list of all catalogued targets is compiled from the ingested FITS tables and compared with the WASP catalogue. New objects are given IAU-compatible names, and all objects are assigned to a $5^\circ \times 5^\circ$ sky tiles based on their coordinates. Photometric data are split from the input files and stored as intermediate per-sky-tiles. Photometric points within each sky-tile are re-ordered to ensure that they are in consecutive rows for a given star. These files are registered within the archive data base management system (DBMS) along with their names, location and various meta-data. The archive can then be interrogated and the photometric data extracted as a single, coherent per-object light curve for longer-term temporal analysis. The object catalogue is expected to increase by $\geqslant 3 \times 10^6$ objects per year. This public archive is hosted at Leicester within Leicester Data base and Archive Service (LEDAS).

3.2 Transit searching

The large number of stars makes visual inspection of every light curve unfeasible. For this reason, the transit-searching programs provide rank ordered lists of the best light curves based on derived transit depth, signal-to-noise ratio, and for periods less than 5 d. Another important and effective parameter in culling the list of candidates was the signal-to-red-noise ratio, ($S_{\rm red}$). $S_{\rm red}$ is the ratio of the best-fitting transit depth to rms scatter and is described in detail in Collier-Cameron et al. (2006). Our refined list of candidates can then be inspected visually for further analysis. Light curves that show unusual extinction variations or other systematic problems can then be eliminated. Once the spurious candidates are culled from the master list, further analysis of the light curves is undertaken.

There are several well-used transit detection algorithms (Tingley 2003; Moutou et al. 2005). These include the box-shaped searches, such as, the box-fitting least-squares (BLS) algorithm (Kovács, Zucker & Mazeh 2002), matched filter algorithms (Kay 1998) and Bayesian techniques (Defaÿ, Deleuil & Barge 2001; Aigrain & Favata 2002). We have applied an improved BLS algorithm to the 2004 data to search for transits. This method is described in detail in a companion paper by Collier-Cameron et al. (2006). BLS allows fast and efficient searching for transits, while keeping the false alarm rate low. Additionally, Moutou et al. (2005) suggest that the BLS method was preferable in a comparison of several commonly used algorithms. An extensive comparison of the leading transit detection algorithms as applied to SW data is currently underway (Enoch et al., in preparation).

Several additional techniques were adopted to the transit finding software to keep the false alarm rate low. These include a test for ellipsoidal variations in the light curve, such as would be produced by close stellar eclipsing binary systems. The amplitude of the ellipsoidal variations, $(S/N)_{\rm ellip}$, is also given for each system. Similar methods applied to OGLE candidates were successful in distinguishing stellar sources from true ESP candidates (Sirko & Paczyński 2003). Additionally, true ESP transit light curves should be flat at the phase 180° away from the transit, at phase 0.5, the 'anti-transit'. Hence, tests for the variability at phase 0.5 (Burke et al. 2006) were also added. We present our results for this set of SW data in the next section. From these and further scrutiny to distinguish low-amplitude stellar systems from true ESPs, we cull our list of ESP candidates.

4 RESULTS

Systems that have good signal-to-noise ratio and transit depths less than 10 per cent are presented in Table 2. Here, we have excluded

Table 2. Light curve data for SW low-amplitude sources.

Name 1SWASP	S_{red}[a]	Period (d)	δ (per cent)	Duration (h)	Epoch[b]	N_{trans}	$\Delta\chi^2$	$(S/N)_{ellip}$[c]
J230808.34+333803.9	21.2	2.23	2.15	2.45	3149.2152	15	1922	7.3
J231240.14+321540.4	12.6	2.53	3.08	2.59	3148.7063	9	969	2.10
J231302.08+262724.3	11.1	4.39	2.16	3.05	3149.1804	7	1188	4.0
J231533.56+232637.5	11.6	3.36	2.89	3.79	3148.7560	10	1597	0.7
J231807.73+240522.1	21.3	2.54	5.96	1.90	3150.5115	8	1281	1.5
J232639.10+233219.2	16.8	2.21	3.67	2.54	3150.3117	15	3405	2.3
J232700.56+200609.1	22.3	3.24	5.79	2.45	3149.3855	11	733	3.2
J233325.17+332632.1	12.4	2.27	1.59	3.34	3150.2111	16	1072	9.2
J234318.41+295556.5	14.4	4.24	2.81	2.42	3151.8626	6	1213	2.9
J000029.25+323300.9	14.0	1.20	2.49	2.35	3151.9736	17	939	7.2
J000233.27+331516.8	15.6	2.37	3.01	2.04	3152.5501	11	1476	10.2
J002040.07+315923.7	11.6	2.52	1.27	3.00	3151.4864	9	287	0.4
J002728.02+284649.2	9.7	1.52	1.22	3.17	3166.9666	12	1136	2.5
J002819.22+335122.1	12.0	3.45	8.07	3.82	3165.2148	6	1033	2.6
J003039.21+205719.1	10.5	2.28	1.91	2.38	3166.6460	9	668	0.4
J004804.21+202258.8	25.2	1.83	6.45	2.71	3167.0060	9	3326	6.6
J005107.84+214352.7	13.7	1.47	4.24	2.42	3167.6596	8	3322	5.9
J005225.90+203451.2	12.4	1.72	2.78	1.66	3166.9509	8	1198	3.7
J005250.45+221038.8	19.7	2.46	6.46	2.30	3167.0449	6	1011	1.6
J005818.26+204348.0	10.8	2.20	8.83	2.54	3167.1818	7	2962	7.0
J010151.11+314254.7	9.6	2.19	1.66	2.64	3167.4457	10	694	3.2
J010553.38+241358.3	8.9	3.35	2.88	1.73	3165.6700	4	305	1.7
J010706.32+313918.0	20.2	4.10	4.54	2.14	3167.5442	4	2569	0.2
J013033.21+311447.0	7.0	4.40	1.56	3.58	3179.5786	3	408	2.3
J013100.45+374745.2	15.6	1.65	3.60	2.14	3181.5542	12	841	0.1
J013250.08+194332.7	10.7	3.13	5.60	4.27	3166.2451	6	1248	2.8
J013452.76+293626.5	11.8	1.91	1.53	3.31	3166.0957	14	1674	1.1
J014400.22+344449.2	11.9	3.72	2.73	3.17	3180.2839	5	914	4.4
J015625.53+291432.5	12.2	1.45	1.24	3.22	3182.5415	13	1084	4.9
J015711.29+303447.7	12.3	2.04	1.55	2.30	3182.5612	9	1253	1.3
J015951.59+354455.4	8.5	1.19	2.28	1.97	3181.9274	13	586	12.9
J020720.96+325526.5	10.1	1.54	4.52	3.22	3181.7719	10	1354	5.8
J021217.50+335319.2	20.0	3.91	6.85	2.64	3180.5364	3	1883	1.0
J022421.03+375419.9	11.3	4.16	5.47	2.81	3191.8221	4	2530	3.3
J022651.05+373301.7	9.6	1.22	1.29	2.02	3194.6500	8	1782	4.3
J023445.65+251244.0	7.6	1.55	2.36	2.62	3194.4315	6	286	1.1
J024206.53+364029.7	16.4	2.59	4.78	2.81	3193.8696	7	763	3.4
J025419.14+324240.7	20.4	2.91	5.11	2.71	3192.4337	4	319	0.4
J025500.31+281134.0	9.0	2.17	3.74	2.76	3191.9254	6	767	1.4
J025712.69+403140.0	9.8	2.22	1.80	2.50	3192.7651	6	549	10.7
J025958.91+294434.6	10.0	1.73	5.41	2.33	3193.1976	6	1010	2.3

[a] S_{red} – signal-to-red-noise ratio(see text).
[b] JD = 245 0005.5 + epoch.
[c] $(S/N)_{ellip}$ – amplitude of ellipsoidal variations (see text).

systems showing secondary eclipses in their light curves and stars with any brighter neighbouring stars within a 48-arcsec radius. We will apply strict criteria to the sources listed in the table to separate the stellar systems from the possible ESPs. Systems likely to be low stellar mass binaries are interesting in their own right and if confirmed would add valuable information to the mass–radius relations for low-mass stars, and are thus included here. However, our current analysis does not allow us to give an accurate estimate of the binary fraction of the SW fields. Our transit-searching methods were optimized for finding transit-like events, and many types of binaries [those with large changes in magnitude (>10 per cent) or large ellipsoidal amplitudes] are not reported. Thus, any estimate would only provide a lower limit to the true binary fraction, and this investigation is left for future publications.

4.1 ESP candidate selection

In the present work, we are interested in the best possible ESP candidates and require these to have (i) high signal-to-noise light curves ($S_{red} > 7$), (ii) a reasonable transit depth for spectral type, (iii) a reasonable transit duration, with $\eta < 1.3$, where η is the ratio of the observed transit duration to that expected based on the stellar and planetary radii (Tingley & Sackett 2005), (iv) a flat-bottomed transit shape, (v) observed for at least three transits and (vi) an ellipsoidal amplitude less than 5. Later-type main-sequence dwarf stars will have deeper eclipses, and transit depths may be as large as 20 per cent. Most hot-Jupiters have periods less than 10 d, which thus limits the transit duration to <7 h (Kane et al. 2005). A grazing angle transiting ESP may show a '*V*-shaped'

Table 3. SW candidate stellar and planetary parameters.

Name 1SWASP	V_{SW}	$V-K$	$J-K$	T_{eff}	Spec. type	$R_\star$ $R_\odot$	R_p R_J	η	Comment
J230808.34+333803.9	10.8	1.41	0.28	6051	F9	1.14	1.43	0.85	Ellip. large
J231240.14+321540.4	11.8	1.46	0.30	5990	G0	1.11	1.66	0.85	R_p too large
J231302.08+262724.3	10.6	3.68	0.87	4170	M0	0.63	0.79	1.19	Giant?
J231533.56+232637.5	11.6	1.72	0.35	5661	G6	0.96	1.39	0.13	ESPc
J231807.73+240522.1	12.0	2.31	0.54	5034	K3	0.76	1.63	0.74	R_p too large
J232639.10+233219.2	11.5	1.26	0.22	6256	F7	1.25	2.04	0.81	R_p too large
J232700.56+200609.1	12.5	1.55	0.29	5870	G2	1.05	2.16	0.73	R_p too large
J233325.17+332632.1	11.1	1.74	0.41	5637	G6	0.95	1.01	1.25	Ellip. large
J234318.41+295556.5	10.7	2.31	0.55	5034	K3	0.76	1.09	0.84	ESPc
J000029.25+323300.9	12.0	2.24	0.57	5101	K2	0.77	1.01	1.29	Ellip. large
J000233.27+331516.8	11.3	1.04	0.29	6573	F4	1.40	2.07	0.60	R_p too large
J002040.07+315923.7	11.8	1.51	0.31	5921	G1	1.08	1.04	1.06	ESPc
J002728.02+284649.2	9.6	2.84	0.71	4602	K5	0.69	0.65	1.72	Giant?/large η
J002819.22+335122.1	12.5	1.52	0.35	5908	G1	1.07	2.39	0.98	R_p too large
J003039.21+205719.1	11.0	1.31	0.55	6186	F8	1.21	1.23	0.92	ESPc
J004804.21+202258.8	10.7	2.08	0.50	5260	K1	0.82	1.78	1.1	Ellip. large
J005107.84+214352.7	11.1	1.51	0.30	5921	G1	1.08	1.90	0.95	R_p too large
J005225.90+203451.2	11.2	1.89	0.46	5465	G9	0.88	1.25	0.71	ESPc
J005250.45+221038.8	12.3	1.47	0.33	5973	G0	1.10	2.38	0.74	R_p too large
J005818.26+204348.0	12.4	1.77	0.38	5602	G7	0.93	2.09	0.63	R_p too large
J010151.11+314254.7	11.1	1.04	0.17	6573	F4	1.40	1.42	1.04	ESPc
J010553.38+241358.3	11.1	1.49	0.33	5947	G1	1.09	1.58	0.53	R_p large
J010706.32+313918.0	10.3	1.55	0.30	5870	G2	1.05	1.91	0.6	R_p too large
J013033.21+311447.0	10.6	1.64	0.34	5758	G4	1.00	1.07	1.08	ESPc
J013100.45+374745.2	11.1	1.35	0.30	6130	F8	1.18	1.90	0.78	R_p large
J013250.08+194332.7	11.4	1.91	0.42	5442	G9	0.87	1.76	0.14	R_p too large
J013452.76+293626.5	10.1	2.68	0.64	4720	K5	0.70	0.40	1.60	Giant/large η
J014400.22+344449.2	11.2	1.30	0.25	6200	F8	1.22	1.72	0.88	R_p too large
J015625.53+291432.5	10.3	2.30	0.54	5044	K3	0.76	0.72	1.67	ESPc?/large η
J015711.29+303447.7	10.4	1.19	0.34	6354	F6	1.30	1.38	0.77	ESPc
J015951.59+354455.4	11.0	3.07	0.73	4453	K7	0.67	0.86	0.08	Ellip. large
J020720.96+325526.5	12.4	2.27	0.65	5072	K2	0.77	1.40	1.51	Ellip. large
J021217.50+335319.2	11.2	2.62	0.67	4767	K5	0.71	1.59	0.92	R_p large
J022421.03+375419.9	10.7	1.70	0.30	5685	G5	0.97	1.94	0.81	R_p too large
J022651.05+373301.7	8.3	0.83	0.11	6896	F1	1.52	1.47	0.74	ESPc
J023445.65+251244.0	12.1	1.86	0.35	5498	G8	0.89	1.17	1.17	ESPc
J024206.53+364029.7	11.8	1.47	0.29	5973	G0	1.10	2.05	0.89	R_p too large
J025419.14+324240.7	11.7	1.61	0.37	5795	G3	1.02	1.97	0.86	R_p too large
J025500.31+281134.0	11.8	2.00	0.45	5344	K0	0.84	1.34	1.29	ESPc
J025712.69+403140.0	10.6	1.13	0.17	6441	F6	1.34	1.53	0.80	Ellip. large
J025958.91+294434.6	12.2	1.57	0.21	5845	G2	1.04	2.11	0.71	R_p too large

transit, but in most cases this shape would indicate a grazing incidence eclipsing stellar system, and these types of transits are further scrutinized.

In order to estimate the size of the transiting planet, the size of the host star must also be determined. Several colour–temperature relations were used to constrain spectral types and stellar temperatures. The V_{SW} and USNO $B1$ and $R1$ magnitude are available for all stars in our sample, and Tycho B and V plus Two-Micron All Sky Survey (2MASS) J, H and K were used when available. Relations between $V_{SW}-K$ and temperature were derived using a coarse grid of V and K colours from a selection of 30 000 stars from Ammons et al. (2006). Subsequently, the stellar radii were determined from the derived stellar temperatures using $J-H$ colours and the relation from Gray (1992). This relation was further optimized with a polynomial fit for the FGKM temperature range. No reddening correction was included in $V_{SW}-K$. In general, with SW observations away from the Galactic plane, the reddening correction should be small, but would serve to increase $V-K$ and artificially lower the derived stellar radii. In Fig. 2, we show a histogram of stellar radii for a sample of ≈2000 stars (ones having all of the appropriate colours) selected from all fields and returned from the transit search code as having 'transit-like' variability. The large peak in the figure at radii between 0.6 and 0.8 $R_\odot$ corresponds to the late K and M0 stars from the faint end of the SW data.

We derived a planet's radius using the estimated stellar radius and a simple geometric transit model. The transit depth, ΔF, is related to the ratio of the area of the planet to that of the star with the equation:

$$\frac{\Delta F}{F} = \left(\frac{R_p}{R_s}\right)^2, \quad (1)$$

where F is the baseline flux of the star, and R_p and R_s are the radius of the planet and star, respectively. Planetary radii in Table 3 are given in units of Jupiter-radii using the above relation from Tingley & Sackett (2005), and the table also includes η.

Additionally, we further refined the spectral type and host star's radii using 2MASS colours to distinguish between dwarfs and

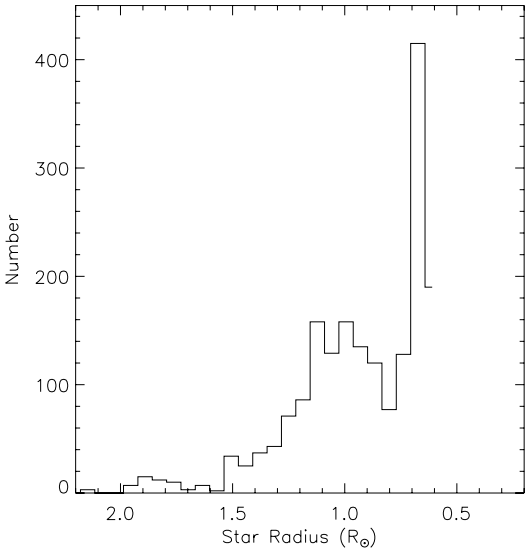

Figure 2. Histogram of stellar radii for a sample of stars from all fields returned from the transit search code (see text).

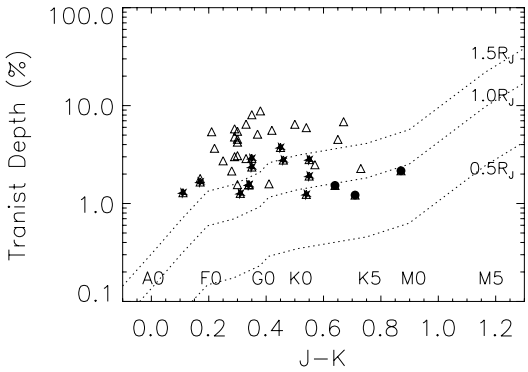

Figure 3. Transit depth plotted as a function of colour indices, $J - K$ for our sample of sources (indicated as open triangles, △), with the most promising 12 candidates from Table 3 over-plotted as filled stars (⋆). The three sources noted as 'Giants' are over-plotted as filled circles. Over-plotted are curves showing the expected transit depth for planets with radii of 0.5, 1.0 and 1.5 R_J (see text).

giants. Similar transit depths for non-main-sequence stars would imply radii larger than that of Jupiter-sized planets. The 2MASS $J - K$ colour index is also presented in Table 3, and we compare the transit depths to infrared colours in Fig. 3. $J - K$ has been shown to be a powerful tool in distinguishing dwarfs from giants (Brown 2003). Values of $J - K > 0.7$ are a strong indication that the star is a giant, and hence the observed transit is caused by a body much larger than a Jupiter-sized ESP. Or, in some cases the giant may be diluting the eclipse of a stellar binary, and also be an imposter. The three sources excluded as 'Giants' are over-plotted with filled circles.

4.2 ESP transit candidates

The above criteria (presented in Section 4.1) were rigorously applied to our selection of the best low-amplitude sources. This leaves us with 12 good ESP candidates. Good ESP candidates are given in italics and commented as *ESPc* in Table 3. Over-plotted in Fig. 3 are the theoretical curves for 0.5, 1.0 and 1.5 Jupiter-radii planets.

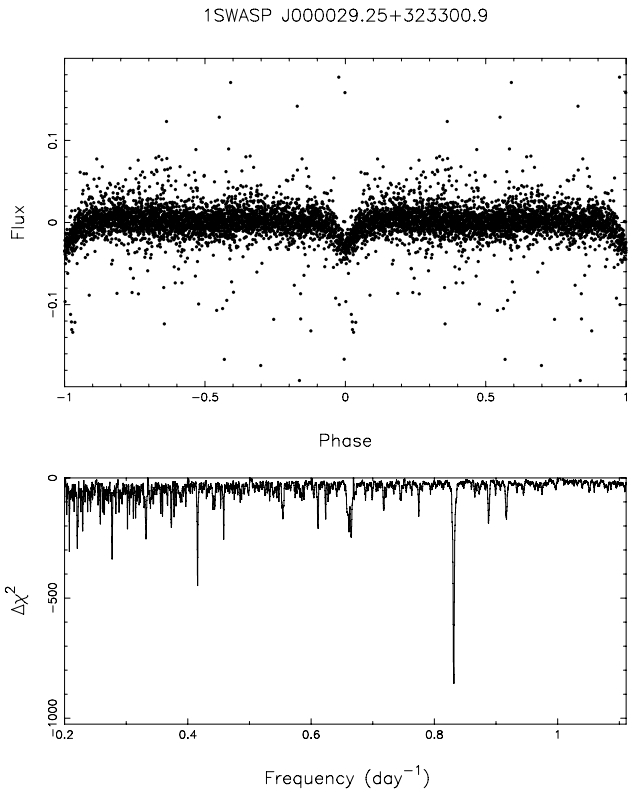

Figure 4. We show sample timing data for sources that were disqualified as ESP candidates because of large ellipsoidal variations. The top panel shows the light curve folded on the best-fitting period, and bottom panel shows the periodogram for 1SWASP J000029.25+323300.9.

It can be seen that many of these source's transits have reasonable planetary radii between 0.5 and 1.5 R_J, and our best candidates are indicated by a filled star (⋆) symbol. Other sources in the figure have large ellipsoidal variation or have large derived planetary radii ($R_p > 1.9\ R_J$), and hence have been eliminated.

We now discuss several of the sources that were not chosen as ESP candidates and those reasons, and we then discuss the properties of the best ESP candidates individually. Light curves and periodograms for these sources are shown in Figs (4–17). Periodograms are included to show the robustness of the period searches and are discussed for unusual cases.

Several sources presented in Table 2 had ellipsoidal amplitudes great than 5, although several of these sources had reasonable planetary radii. We eliminated these as ESP candidates and these are noted as *Ellip. large* in Table 3. *1SWASP J000029.25+323300.9* and *1SWASP J230808.34+333803.9* are two such sources and their folded light curves and periodograms are shown in Figs 4 and 5.

Three sources that had derived planetary radii below 0.8 R_J and also passed most criteria, including a low ellipsoidal magnitude, but may very well be giant and not dwarf stars. These three stars, *1SWASP J002728.02+284649.2, 1SWASP J013452.76+293626.5* and *1SWASP J231302.08+262724.3*, have $J - K$ greater than ≈0.7. These stars also have very large values for η, and this may also indicate the object causing the transit is indeed stellar.

1SWASP J002040.07+315923.7: a total of nine transits were detected for this system, and the periodogram shows a well-determined period of 2.55 d (Fig. 6). We classify this as a G1 star using

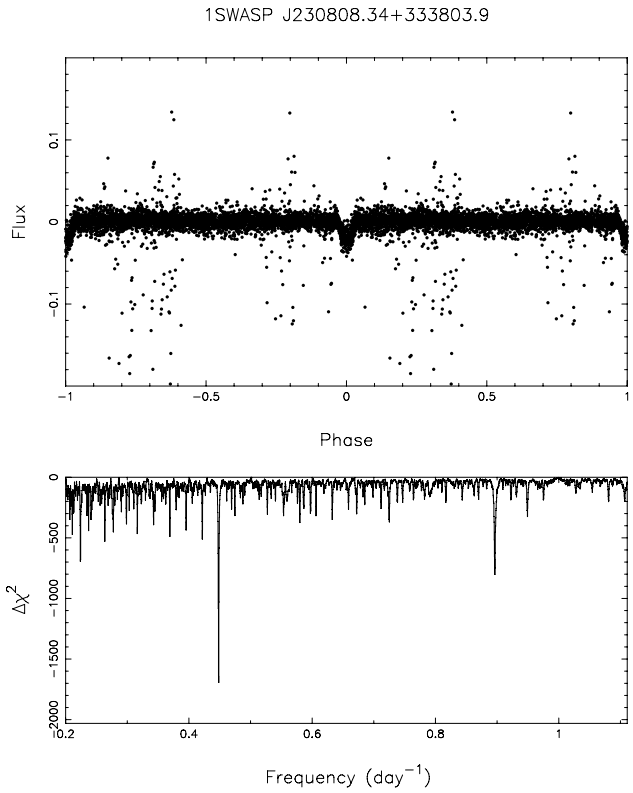

Figure 5. Same as Fig. 4 for 1SWASP J230808.34+333803.9.

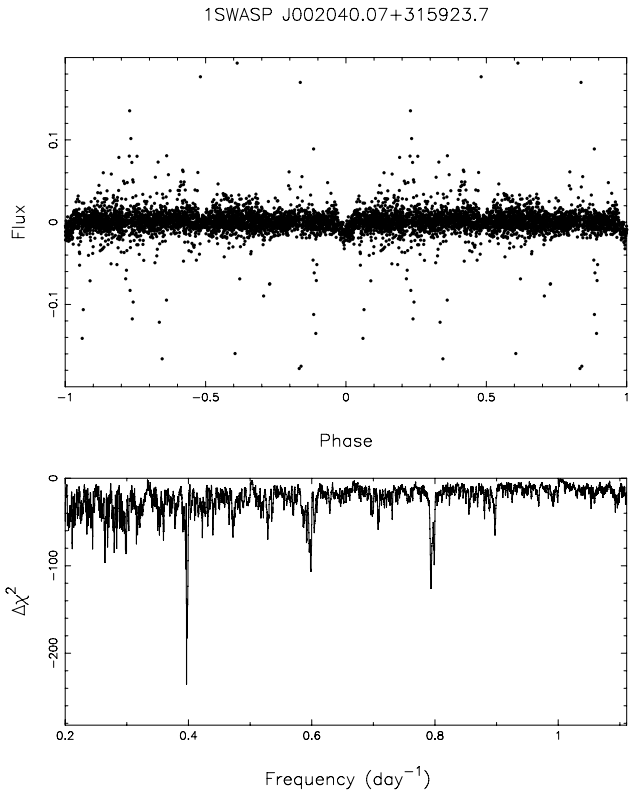

Figure 6. Timing data for the ESP candidate 1SWASP J002040.07+315923.7. The top panel shows the light curve folded on the best-fitting period, and bottom panel shows the periodogram.

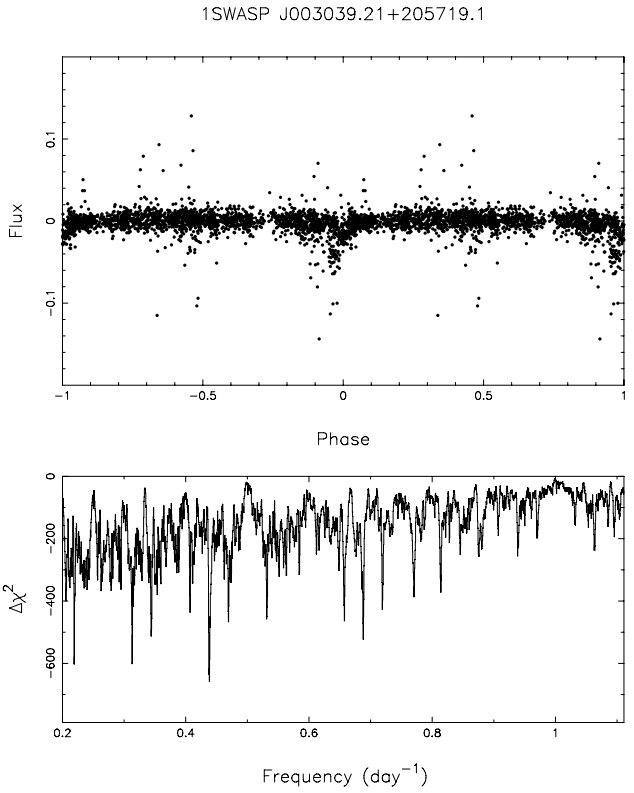

Figure 7. Timing data for the ESP candidate 1SWASP J003039.21+205719.1. Details are the same as for Fig. 6.

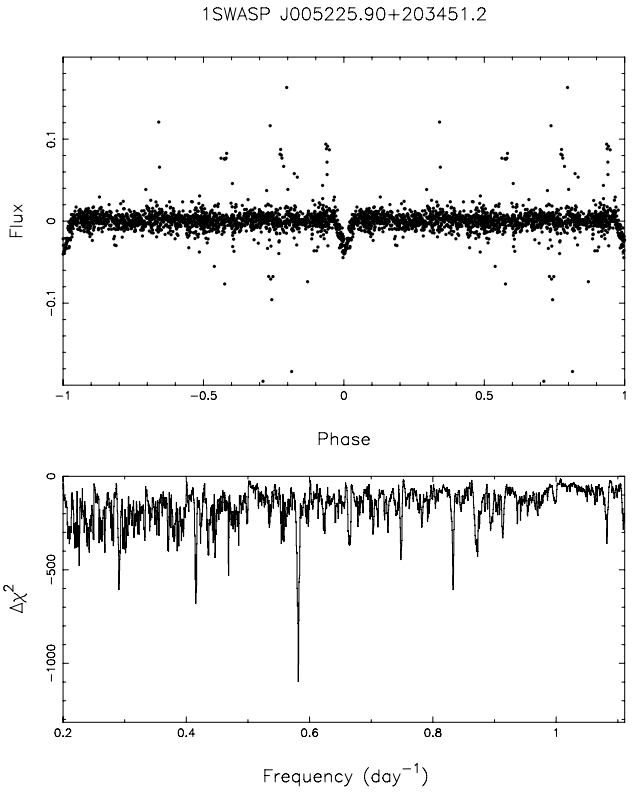

Figure 8. Timing data for the ESP candidate 1SWASP J005225.90+203451.2. Details are the same as for Fig. 6.

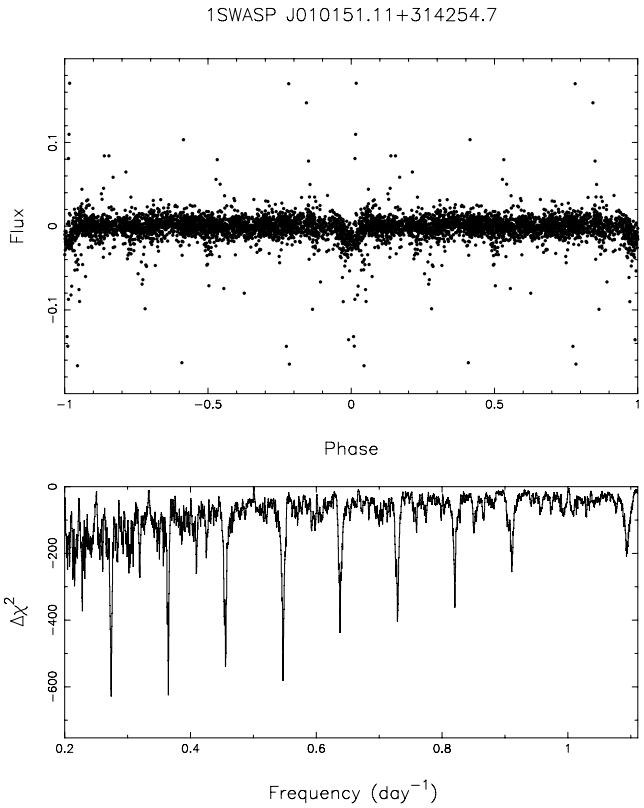

Figure 9. Timing data for the ESP candidate 1SWASP J010151.11+314254.7. Details are the same as for Fig. 6.

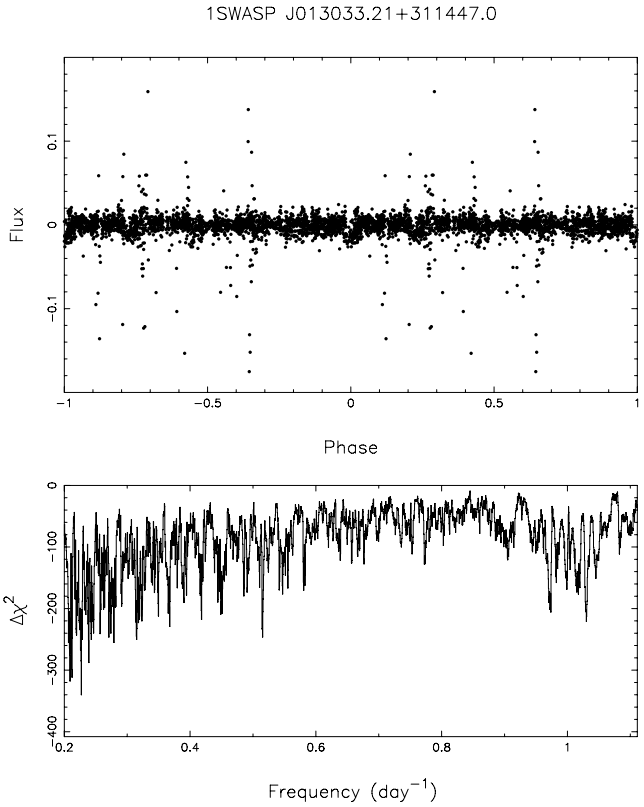

Figure 10. Timing data for the ESP candidate 1SWASP J013033.21+311447.0. Details are the same as for Fig. 6.

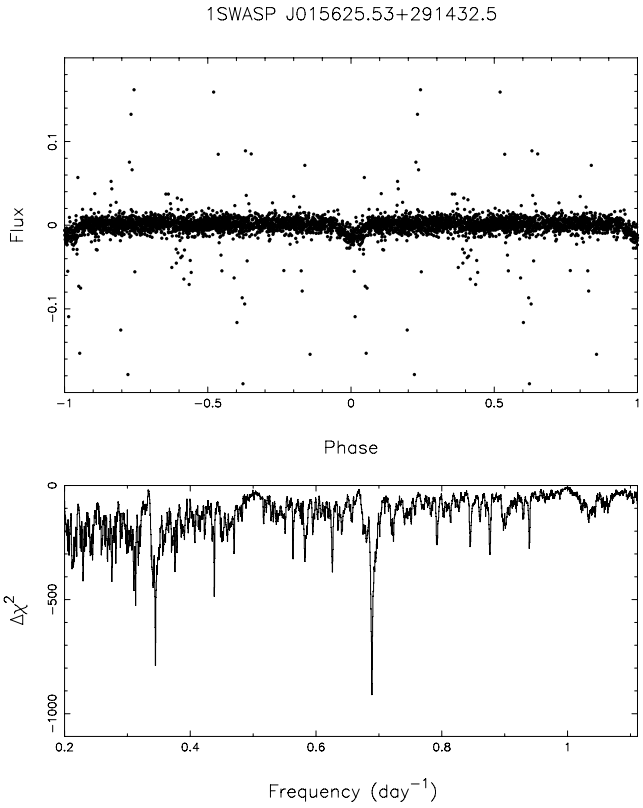

Figure 11. Timing data for the ESP candidate 1SWASP J015625.53+291432.5. Details are the same as for Fig. 6.

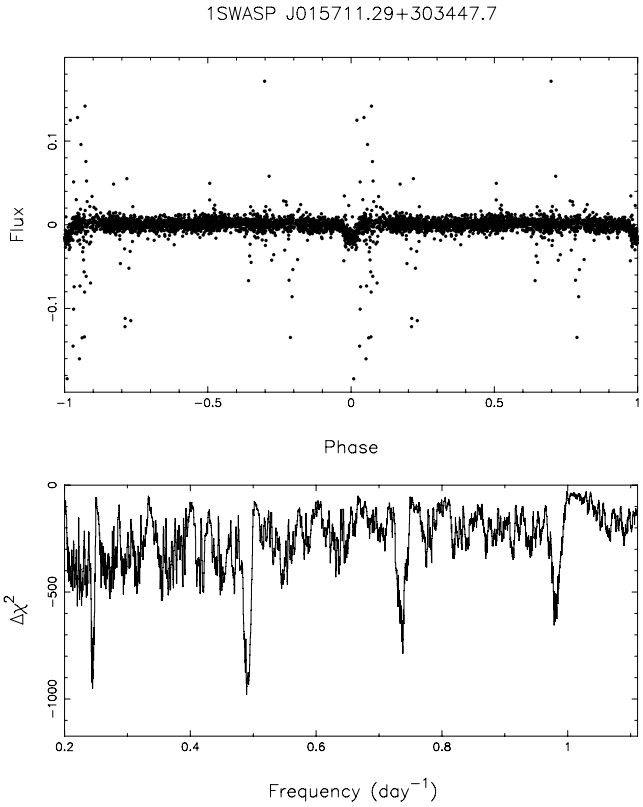

Figure 12. Timing data for the ESP candidate 1SWASP J015711.29+303447.7. Details are the same as for Fig. 6.

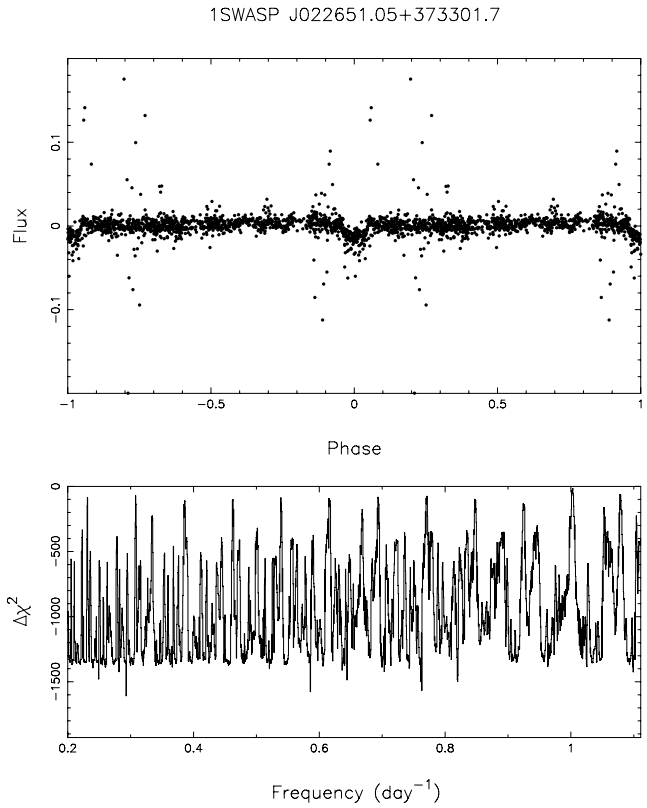

Figure 13. Timing data for the ESP candidate 1SWASP J022651.05+373301.7. Details are the same as for Fig. 6.

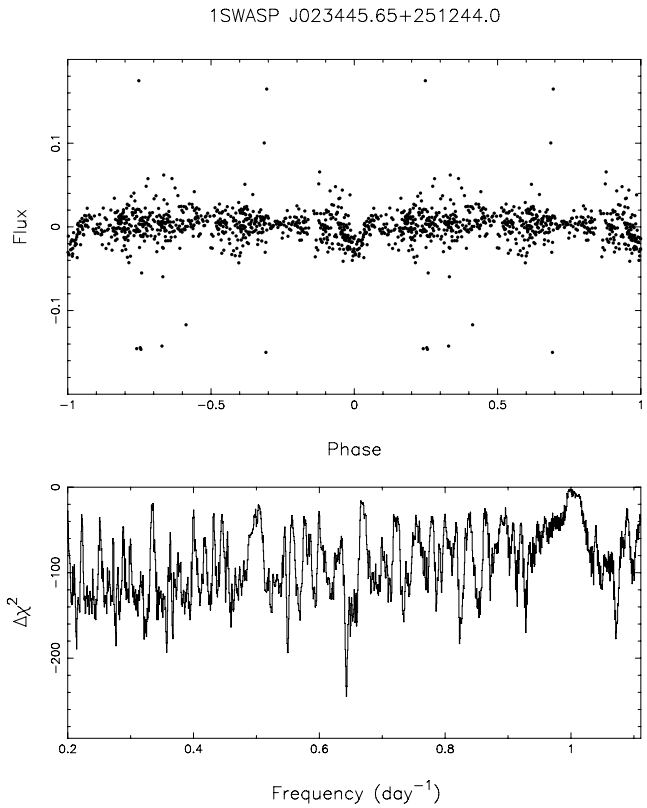

Figure 14. Timing data for the ESP candidate 1SWASP J023445.65+251244.0. Details are the same as for Fig. 6.

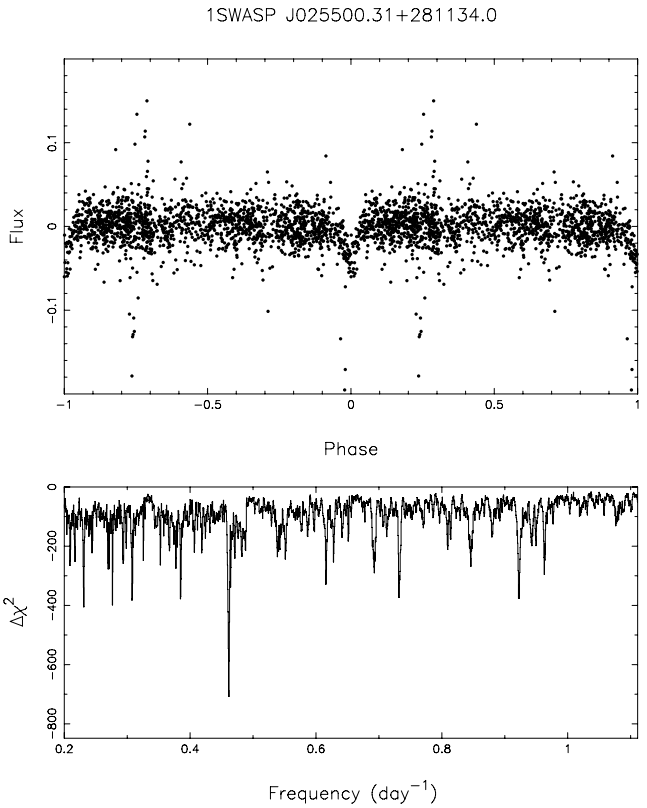

Figure 15. Timing data for the ESP candidate 1SWASP J025500.31+281134.0. Details are the same as for Fig. 6.

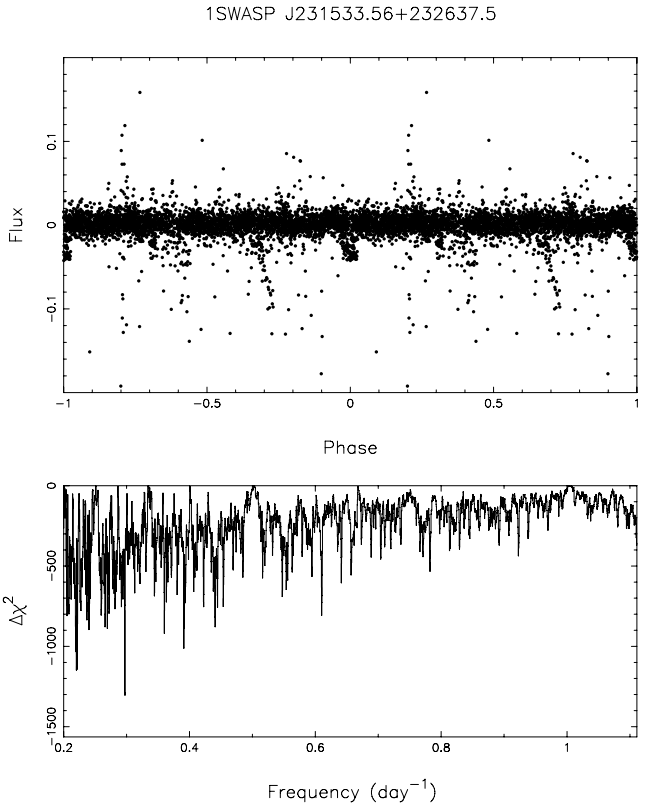

Figure 16. Timing data for the ESP candidate 1SWASP J231533.56+232637.5. Details are the same as for Fig. 6.

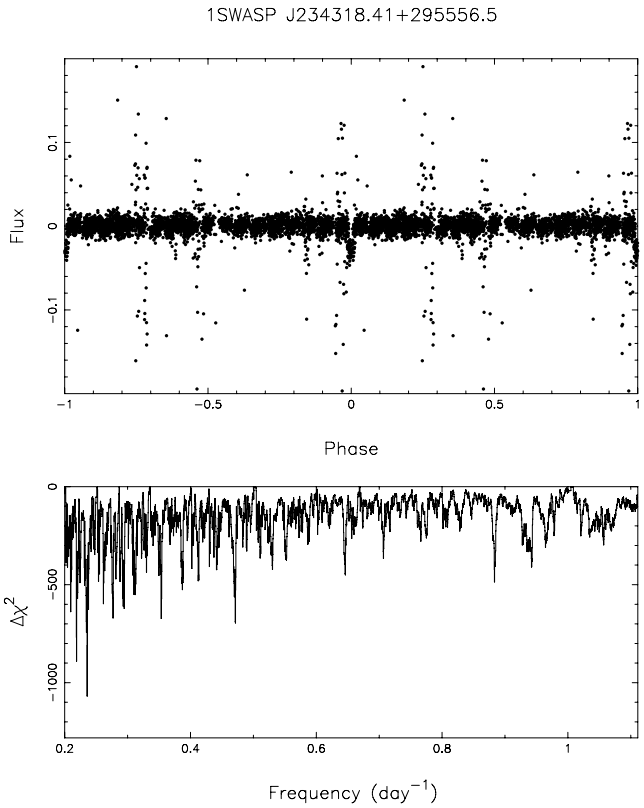

Figure 17. Timing data for the ESP candidate 1SWASP J234318.41+295556.5. Details are the same as for Fig. 6.

colour and temperature relations. This gives a planet radius of 1.2 R_J. Although the transit is clearly visible in its light curve, there are several faint sources within the SW aperture, and blending cannot be ruled out.

1SWASP J003039.21+205719.1, *1SWASP J005225.90+203451.2* and *1SWASP J010151.11+314254.7* were each observed by two different cameras. Although their light curves and periodograms show some scatter, nearly identical transit depths and periods were derived for each star from both of their observations. Their folded light curve and timing information are shown in Figs 7–9. The planetary radii derived for these objects range from 1.2 to 1.4 R_J, and the latter two stars have ellipsoidal amplitudes slightly greater than 3, and these may indeed be stellar systems. However, their ratios of the observed to theoretical transit durations (η) are reasonable.

With a period of 4.4 d, *1SWASP J013033.21+311447.0* is one of the longer period candidates. Although its folded light curve shows a well-defined transit, its periodogram (Fig. 10) has excess scatter, and additional photometric data would be beneficial. We derived a reasonable planetary radius of 1.07 R_J for its G4 spectral type.

1SWASP J015625.53+291432.5: the observed short period for this system (1.45 d) may place it in the class of *very-hot-Jupiters*. Its periodogram, showing a well-defined period, and light curve are presented in Fig. 11. However, the transit depth is relatively shallow for a 0.7 R_J planet and it has a large η, making it more likely to be a grazing incident eclipsing stellar system or diluted by another star. There is another object within the SW aperture making the latter scenario more likely. We note this as a marginal ESP candidate.

1SWASP J015711.29+303447.7: the light curve for this system is flat with a well-pronounced transit (Fig. 12). We derived a planet radius of 1.37 R_J for its derived spectral type of F6. The expected transit duration is reasonable and this is a good ESP candidate worth further follow-up.

1SWASP J022651.05+373301.7: the short period of 1.2 d (Fig. 13) may make this a *very-hot-Jupiter*, but its periodograms show excess scatter and additional photometric measurements are needed to improve the period determination. This source may also be a low-mass stellar system based on its large ellipsoidal amplitude (4.3). Its derived spectral type of F1 for this star results in a large planet of nearly 1.5 R_J. It is one of the most interesting systems that will be followed up spectroscopically.

1SWASP J023445.65+251244.0 has a moderate amount of scatter in its light curve, but the transit is well pronounced (Fig. 14). The transit depth and spectral types result in similar-sized planets of $\approx$1.2 R_J. The expected transit duration is near the higher end for acceptable values ($\eta \approx 1.2$), and further observations are needed to secure this source as ESP and possible very-hot-Jupiter.

1SWASP J025500.31+281134.0 shows a moderate amount of scatter in its light curve (Fig. 15), but does have a well-defined period (2.2 d) and transit (3.7 per cent). This transit depth is one of the larger for ESP candidates and results in a planet radius of 1.3 R_J for a spectral type of K0. The slight '*V*' shape to the transit profile and large value of the expected transit duration ($\eta = 1.3$) may indicate that this is a stellar system.

1SWASP J231533.56+232637.5 and *1SWASP J234318.41+295556.5* have a moderate amount of scatter in their light curves, but the transits are well pronounced for both systems (Figs 16 and 17). Their transit depths and spectral types result in similar-sized planets of $\approx$1.1 and 1.4 R_J, respectively. 1SWASP J234318.41+295556.5 has an ellipsoidal amplitude of 2.9, and may be a stellar binary.

5 DISCUSSION

The majority of candidates found with low-amplitude periodic variability showed obvious signatures of being stellar binaries. We have selected only 12 as new ESP candidates. There are many different types of stellar systems and chance alignments that can show behaviour mimicking a planet's transit. Such possibilities have been separated into three groups (see e.g. Brown 2003): (i) grazing incidence stellar binary systems, (ii) stellar systems consisting of both high- and low-mass stars and (iii) an eclipsing stellar system in which some light from a foreground or background star contaminates the light from the binary reducing the depth of the eclipse and making it appear more 'transit-like'. We have scrutinized our sample of low-amplitude variables with the techniques outlined in Section 3.2, and attempted to eliminate systems from above categories (i) and (ii). However, previous studies on ESPs have shown that it is difficult to remove the third category of false-positive transiting system, the diluted stellar binary (Torres et al. 2005; O'Donovan et al. 2006). For this reason, high-resolution optical spectroscopy is needed to measure RVs for our candidates and determine the companion's mass. Such follow-up has been successful in identifying nearly six such sources from OGLE sample (Konacki et al. 2003, 2004; Bouchy et al. 2004; Pont et al. 2004; Konacki et al. 2005) and is being undertaken by our consortium.

5.1 Expected numbers of ESP

For our sample of 900 000 stars, we are left with $\approx$400 000 that are brighter than $V = 13.5$ and for which SW is statistically sensitive to detect a transiting ESP. If we conservatively estimate only 50 per cent of these stars are late-type (F–M) dwarfs, this reduces our sample size to $\sim$200 000 stars. If 1 per cent of these have

hot-Jupiter companions (Lineweaver & Grether 2003), and we expect 10 per cent of these to show transits (Horne 2003), we therefore should have detected ≈200 ESPs, although this estimate is affected by the true coverage for a particular field. For this reason, we have also estimated the expected fraction of transits recovered for each observed field as a function of transit period and for different numbers of transits. These expected transit yields are shown in Figs 18(a)–(c) for the recovery of two, four and six transits. For sources with periods ⩽5 d and for fields that were observed for 80 or more nights, two transits would have been detected ≈95 per cent of the time. For the fields with poorest coverage, the recovered fraction only drops to ≈80 per cent. However, if we require the recovery of four transits, the recovered fraction is reduced to ≈40 per cent for fields that were observed for at least 80 nights, and ≈10–20 per cent for fields with ⩽60 nights of coverage. The majority of the fields presented here were observed for at least 60 nights, and hence we should recover two transits for ≈80 per cent of the planets present, leading to an expectation of 160 ESPs detected. If we require the recovery of four transits, then this number is reduced to ≈80.

The plethora of short-period ESPs that was predicted in the mid-1990s and recently (Horne 2003) has not come to fruition. Surveys that concentrate on wide fields and brighter stars have only two transit ESP discoveries (TrES-1, Alonso et al. 2004, and XO-1b, McCullough et al. 2006). The majority of other transiting ESPs (six) have come from the OGLE micro-lensing survey of the Galactic Centre and fields nearby (Udalski et al. 2004). Brown (2003) estimated the detection rate for giant ESP including the probability both of a star having a planet and of observing it. This provides an estimate of ≈1 ESP per 25 000 stars. Photometric surveys of open clusters (OCs) with 2- to 4-m class telescopes that observe to much fainter magnitudes [e.g. Street et al. (2003); EXPLORE, van Braun et al. (2005); PISCES, Mochejska et al. (2005, 2006)] have also failed to detect short-period ESPs. These surveys have monitored tens of thousands of stars for tens of days with high precision and to very faint magnitudes ($R \sim 20$), yet found few to no ESPs.

A trend has been established where ESP are found predominately with metal-rich host stars (Santos et al. 2003; Fischer & Valenti 2005). The lack of ESP transit candidate detections in metal-poor globular cluster, 47 Tuc (Gilliland et al. 2000; Weldrake et al. 2005), is consistent with this. Given that these deep OC surveys are sensitive to short-period ESPs, the lack of detections might imply that the frequency of transiting hot-Jupiters is closer to 1 in 50 000 stars. Our present results of 12 ESP candidates in nearly 400 000 stars are consistent with the current detection rates.

There may be several contributing factors to this lack of detections. The weather can seriously diminish the observing duration and shorten the observing window used in many of the estimated ESP yields. Changes in extinction can be difficult to remove from the observations and cause false variability. Additionally, intrinsic stellar variability, especially in stars of later spectral types, may hide the transit signature. Later-type stars will have deeper transit depths and these are more easily recovered for fainter stars. For these reasons, we may then consider if the periodic nature of the transit signal would allow us to recover shallower transit depths or transits from stars fainter than ≈13th magnitude. Periodic signals are most readily recovered from the transit-searching algorithm, but we are ultimately limited by the signal-to-noise ratio and duration of the data. Simulations for the fraction of transits recovered based on each of our field's observing windows have shown that there are several integer periods where the probability of recovering a transit is greatly reduced because of the lack of coverage (e.g. Figs 18a–c), and there also are several periods where the chance for detection is actually increased (see Fig. 18a; $N_{\rm tr} = 6$ case and P = 3 d). In a companion paper, Smith et al. (2006) investigate the effects of the noise properties on transit recovery in the SW data and conclude the best way to reduce the covariant noise is to increase the observing baseline.

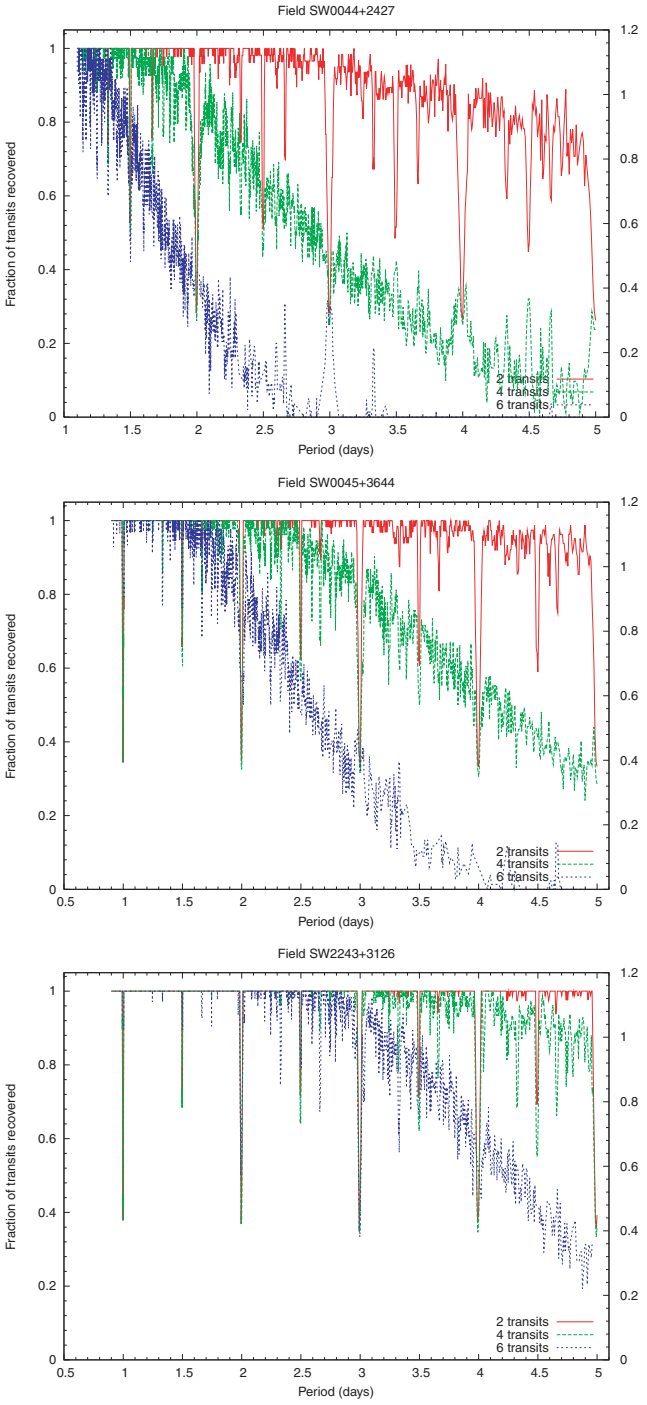

Figure 18. The expected fraction of transits recovered as a function of period and for the detection of two, four and six transits. We show the expected fraction recovered for three fields: (i) 0044+2427, (ii) 0045+3644 and (iii) 2243+3126, representing coverages of ≈30, 80 and over 100 nights, respectively.

Many improvements to the analysis of photometric transit data have been made, and there are additional tests to distinguish stellar

systems from true ESPs (e.g. Tingley & Sackett 2005). The ESP detection rate of the WASP project is presently unknown, but continued SW-N and SW-S observations will discover more high-quality ESP candidates. However, it is important to have spectroscopic follow-up to determine the mass function of these systems. It may be left to space-borne missions, such as Kepler and Convection, Rotation and planetary Transits (COROT), without the hindrance of the atmosphere, to truly determine the frequency of hot-Jupiter and even Earth-size ESPs.

6 CONCLUSIONS

We have presented 41 low-amplitude variables from the SW-N 2004 observing season. From this list, we identified 12 ESPs candidates with periods of 1.2–4.4 d. These have transit depths ≈1–4 per cent implying planetary radii of 1.0–1.5 R_J for their derived spectral types. High-resolution optical spectroscopy to measure RVs and to obtain orbital solutions and masses for these systems is needed to confirm these candidates are true ESPs. Such observations are being undertaken by our consortium. SW-N and SW-S both continue to operate for the 2006 observing season, and with a full eight-camera complement, and are expected to obtain more than twice the amount of data as the 2004 campaign.

ACKNOWLEDGMENTS

The WASP consortium consists of representatives from the Queen's University Belfast, University of Cambridge (Wide Field Astronomy Unit), Instituto de Astrofísica de Canarias, Isaac Newton Group of Telescopes (La Palma), University of Keele, University of Leicester, The Open University and the University of St. Andrews. The SW-N and SW-S instruments were constructed and operated with funds made available from Consortium Universities and the Particle Physics and Astronomy Research Council. SW-N is located in the Spanish Roque de Los Muchachos Observatory on La Palma, Canary Islands which is operated by the Instituto de Astrofísica de Canarias (IAC). We thank an anonymous referee for suggested improvements, and acknowledge useful scientific discussion with I. Dino, J. Smoker and C. Snodgrass. We are grateful to PPARC for financial support.

NOTE ADDED IN PROOF

The official designation for WASP-discovered objects is the identifier of the form 1SWASP J230808.34+333803.9. Since this is unwieldy for frequent use, we are also adopting the short form WASP-*n* (where *n* is a sequential number) for all WASP-discovered transitors in which the transit is confirmed to be caused by a sub-stellar companion (planet or brown dwarf). Anyone confirming WASP discoveries and wishing to use the short form as an alternative to the full identifier is welcome to contact the WASP consortium at wasp-steer@astro.le.ac.uk to assign a WASP-*n* number.

REFERENCES

Aigrain S., Favata F., 2002, A&A, 395, 625
Alonso R. et al., 2004, ApJ, 613, L153
Ammons S. M., Robinson S. E., Strader J., Laughlin G., Fischer D., Wolf A., 2006, ApJ, 638, 1004
Bouchy F., Pont F., Santos N. C., Melo C., Mayor M., Queloz D., Udry S., 2004, A&A, 421, L13
Bouchy F., Pont F., Melo C., Santos N. C., Mayor M., Queloz D., Udry S., 2005a, A&A, 431, 1105
Bouchy F. et al., 2005b, A&A, 444, L15
Brown T., 2003, ApJ, 593, L125
Burke C. J., Gaudi B. S., Depow D. L., Pogge R. W., 2006, AJ, submitted
Butler R. P. et al., 2006, ApJ, 646, 505
Charbonneau D., Brown T. M., Latham D. W., Mayor M., 2000, ApJ, 529, L45
Collier Cameron A. et al., 2006, MNRAS, in press (astro-ph/0609418)
Defaÿ C., Deleuil M., Barge P., 2001, A&A, 365, 330
Fischer D. A., Valenti J., 2005, ApJ, 622, 1102
Gilliland R. et al., 2000, ApJ, 545, L47
Gray D. F., 1992, The Observation and Analysis of Stellar Photospheres. Cambridge Univ. Press, Cambridge
Henry G. W., Margy G. W., Butler R. P., Vogt S. S., 2000, ApJ, 529, L41
Holman M. J. et al., 2006, ApJ, in press (astro-ph/0607571)
Horne K., 2003, in Deming D., Seager S., eds, ASP Conf. Ser. Vol. 294, Scientific Frontiers in Research on Extrasolar Planets. Astron. Soc. Pac., San Francisco, p. 361
Jayawardhana R., Fisher S., Hartmann L., Telesco C., Pina R., Fazio G., 1998, ApJ, 503, L79
Kane S. R., Collier Cameron A., Horne K., James D., Lister T. A., Pollacco D. L., Street R. A., Tsapras Y., 2004, MNRAS, 353, 689
Kane S. R., Collier Cameron A., Horne K., James D., Lister T. A., Pollacco D. L., Street R. A., Tsapras Y., 2005, MNRAS, 364, 1091
Kay S., 1998, Fundamentals of Statistical Signal Processing: Detection Theory. Prentice-Hall PTR, Upper Saddle River
Konacki M., Torres G., Jha S., Sasselov D., 2003, Nat, 421, 507
Konacki M. et al., 2004, ApJ, 609, L37
Konacki M., Torres G., Sasselov D. D., Jha S., 2005, ApJ, 624, 372
Kovács G., Zucker S., Mazeh T., 2002, A&A, 391, 369
Lecavelier Des Etangs A. et al., 1997, A&A, 325, 228
Lineweaver C. H., Grether D., 2003, ApJ, 598, 1350
Marcy G. W., Butler R. P., 1998, ARA&A, 36, 57
Marcy G., Butler R. P., 2000, PASP, 112, 137
Mayor M., Queloz D., 1995, Nat, 378, 355
McCullough et al., 2006, ApJ, in press (astro-ph/0605414)
Mochejska B. J. et al., 2005, AJ, 129, 2856
Mochejska B. J. et al., 2006, AJ, 131, 1090
Moutou C. et al., 2005, A&A, 437, 355
O'Donovan F. T. et al., 2006, ApJ, 644, 1237
Pollacco D. L. et al. 2006, PASP, in press (astro-ph/0608454)
Pont F., Bouchy F., Queloz D., Santos N. C., Melo C., Mayor M., Udry S., 2004, A&A, 426, L15
Robin A. C., Reylé C., Derriére S., Picaud S., 2003, A&A, 409, 523
Santos N. C., Israelian G., Mayor M., Udry S., 2003, A&A, 398, 363
Sirko E., Paczyński B., 2003, ApJ, 592, 1217
Smith B. A., Terrile R. J., Sci, 226, 1421
Smith A. M. S. et al., 2006, MNRAS, in press (astro-ph 0609618)
Street R. A. et al., 2003, MNRAS, 340, 1287
Tamuz O., Mazeh T., Zuckerm S., 2005, MNRAS, 356, 1466
Tingley B., 2003, A&A, 403, 329
Tingley B., Sackett P. D., 2005, ApJ, 627, 1011
Torres G., Konacki M., Sasselov D. D., Jha S., 2005, ApJ, 619, 558
Tyson N. D., Gal R., 1993, AJ, 105, 1206
Udry S. et al., 2000, A&A, 356, 590
Udalski A., Szymanski M. K., Kubiak M., Pietrzynski G., Soszynski I., Zebrun K., Szewczyk O., Wyrzykowski L., 2004, Acta Astron., 54, 313
von Braun K., Lee B. L., Seager S., Yee H. K. C., Mallén-Ornelas G., Gladders M. D., 2005, PASP, 117, 141
Weldrake D. T. F., Sackett P. D., Bridges T. J., Freeman K. C., 2005, ApJ, 620, 1043
Wilson D. M. et al., 2006, PASP, in press (astroph/0607591)

This paper has been typeset from a TEX/LATEX file prepared by the author.